Extending the limits of powder diffraction analysis: Diffraction parameter space, occupancy defects, and atomic form factors
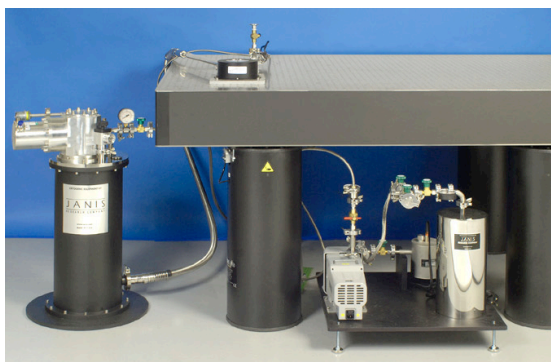
Liang Yin, Gerard S. Mattei, Zhou Li, Jianming Zheng, Wengao Zhao, Fredrick Omenya, Chengcheng Fang, Wangda Li, Jianyu Li, Qiang Xie, Ji-Guang Zhang, M. Stanley Whittingham, Ying Shirley Meng, Arumugam Manthiram, and Peter G. Khalifah

Extending the limits of powder diffraction analysis: Diffraction parameter space, occupancy defects, and atomic form factors

Liang Yin,[1,2] Gerard S. Mattei,[1,2] Zhou Li,[1,2] Jianming Zheng,[3] Wengao Zhao,[3]
Fredrick Omenya,[4] Chengcheng Fang,[5] Wangda Li,[6] Jianyu Li,[6] Qiang Xie,[6]
Ji-Guang Zhang,[3] M. Stanley Whittingham,[4] Ying Shirley Meng,[5] Arumugam Manthiram,[6]
and Peter G. Khalifah[1,2,a)]

[1]*Department of Chemistry, Stony Brook University, Stony Brook, New York 11794, USA*
[2]*Chemisty Division, Brookhaven National Laboratory, Upton, New York 11973, USA*
[3]*Energy and Environment Directorate, Pacific Northwest National Laboratory, Richland,
Washington 99354, USA*
[4]*Department of Chemistry, Binghamton University, Binghamton, New York 13902, USA*
[5]*Department of NanoEngineering, University of California San Diego, La Jolla, California 92093, USA*
[6]*Materials Science and Engineering Program and Texas Materials Institute, The University of Texas at Austin,
Austin, Texas 78712, USA*

Although the determination of site occupancies is often a major goal in Rietveld refinement studies, the accurate refinement of site occupancies is exceptionally challenging due to many correlations and systematic errors that have a hidden impact on the final refined occupancy parameters. Through the comparison of results independently obtained from neutron and synchrotron powder diffraction, improved approaches capable of detecting occupancy defects with an exceptional sensitivity of 0.1% (absolute) in the class of layered NMC ($Li[Ni_xMn_yCo_z]O_2$) Li-ion battery cathode materials have been developed. A new method of visualizing the diffraction parameter space associated with crystal-lographic site scattering power through the use of f^* diagrams is described, and this method is broadly applicable to ternary compounds. The f^* diagrams allow the global minimum fit to be easily identified and also permit a robust determination of the number and types of occupancy defects within a structure. Through a comparison of neutron and X-ray diffraction results, a systematic error in the synchrotron results was identified using f^* diagrams for a series of NMC compounds. Using neutron diffraction data as a reference, this error was shown to specifically result from problems associated with the neutral oxygen X-ray atomic form factor and could be eliminated by using the ionic O^{2-} form factor for this anion while retaining the neutral form factors for cationic species. The f^* diagram method offers a new opportunity to experimentally assess the quality of atomic form factors through powder diffraction studies on chemically related multi-component compounds. *Published by AIP Publishing.*
https://doi.org/10.1063/1.5044555

I. INTRODUCTION

Powder diffraction is perhaps the most widely used analytical technique in the field of materials chemistry. The utility and importance of powder diffraction methods for structural analysis are reflected in the prevalence of powder diffraction facilities at neutron and synchrotron user facilities and in the very high publication rates at these beamlines. The most basic level of structural analysis using powder diffraction data includes both the determination of lattice parameters and the fingerprint analysis of peak positions and intensities for phase identification, and both of these techniques can be readily carried out on a laboratory X-ray powder diffractometer. However, a deeper level of structural analysis can be accomplished through Rietveld refinement, a method in which the crystal structure of a material is determined by optimizing a structural model so that the peak positions, peak shapes, and peak intensities calculated from this model best match the experimentally measured data.

The use of powder diffraction data collected at neutron and synchrotron sources is essential for extracting the highest quality structural data using the Rietveld method as these data can have numerous advantages over conventional laboratory X-ray data, including access to data spanning a much wider range in d and Q, a superior signal/noise ratio, better resolution of diffraction peaks, more precise determination of peak positions, less of a need for correction for experimental aberrations such as absorption or preferred orientation, and the potential to measure the sample under conditions where the atomic form factors provide greater sensitivity to key structural questions. For the last of these, neutron diffraction data offer two key advantages including the ability of low-Z atoms to act as strong scatters (especially in the case of oxygen, which is a key component of many functional materials) and a minimal reduction in the loss of intensity at low-d/high-Q due to the scattering occurring from a strongly localized nucleus (rather than from the poorly localized electron cloud responsible for X-ray scattering).

Although the Rietveld refinement of powder diffraction data from neutron and synchrotron sources in theory has the

---

potential to determine structural models with exquisite sensitivity to crystallographic parameters based on the estimated standard deviations (esds) for these parameters, in practice it is found that there are very large systematic errors in the determination of some key parameters, especially the site occupancies and atomic displacement parameters (ADPs). These problems are most obvious when comparisons are made between the two structural models that are obtained from a single sample when neutron and synchrotron powder diffraction data from the sample are independently utilized for refinements. In this work, it will be shown that with the proper methods for analyzing data, superb agreement (~0.1% absolute) in occupancy-related parameter values can be obtained between structural models refined using neutron and synchrotron data. It is found that the powder diffraction data from modern user facility beamlines are of sufficient quality to allow systematic problems in the standard neutral atomic form factors used in X-ray diffraction data to be discerned. This discrimination is best accomplished using a new method that is described for the first time here for visualizing diffraction parameter space using f^* diagrams in which the relative scattering powers of the different crystallographic sites in a structure and their sensitivities to different site occupancies are visualized. In this work, these methods have been applied to quantify occupancy defects in layered NMC ($Li[Ni_xMn_yCo_z]O_2$) compounds with the general formula of $Li(Ni_xMn_yCo_z)O_2$ that belong to the α-NaFeO$_2$ structure type. These methods are most directly applicable to the study of ternary oxides, structure types with 3 independent crystallographic sites, though they can be more broadly generalized to other compounds in a close analogy to pseudo-ternary phase diagrams.

II. EXPERIMENTAL

A total of 14 NMC samples with 10 different nominal compositions were obtained from a variety of sources. Some were obtained from industrial suppliers. Others were synthesized within academic research laboratories. The details of these sample nominal compositions and their synthesis conditions are given in Table S1. Samples had only trace impurities (Fig. S1) which were neglected in Rietveld analyses due to their small amount and minimal overlap with NMC phases.

Laboratory X-ray powder diffraction data for preliminary analyses were collected on a Bruker Advance D8 diffractometer using Cu K_α radiation from a fine focus X-ray tube ($K_{\alpha1}$ = 1.540 592 90(50) Å, $K_{\alpha2}$ = 1.544 427 40(50) Å). The system was operated in a flat plate geometry using a zero-background Si sample holder at a 217.5 mm working radius utilizing a 1D position-sensitive LynxEye Si detector with 192 channels. Data were collected between 8° and 100° with a step size of 0.02°/step and a scan speed of 2 s/step. High resolution synchrotron X-ray powder diffraction data were collected at the 11-BM beamline[1] at the Advanced Photon Source (APS) of Argonne National Laboratory (λ = 0.412721 Å, 0.414576 Å, 0.412688 Å, or 0.457658 Å). Samples were loaded in 0.8 mm Kapton capillaries (Cole-Parmer; 1/32 in. ID and 1/30 in. OD). Experimental tests showed that the capillary loading typically resulted in a 48% (±2%) packing density, a value which was used to calculate an absorption cross section and

to apply a cylindrical absorption correction for all synchrotron samples. Structures were refined using the Rietveld method as implemented in the TOPAS software package (Bruker-AXS, version 6) across a d-spacing range of 5.0 Å–0.5 Å.

Time-of-flight (TOF) neutron powder diffraction experiments were performed on the NOMAD diffractometer[2] at the Spallation Neutron Source (SNS), Oak Ridge National Laboratory (ORNL) during the 2017-A run cycle. About 100 mg of powder were packed in a 3 mm diameter fused quartz capillary from Charles Supper Company, and typical data acquisition times of 100 min were used. NOMAD data were normalized against a vanadium rod and reduced using custom beamline software written using the IDL programming language. The neutron coherent scattering lengths (Li: −1.90 fm, Ni: 10.3 fm, Mn: −3.73 fm, Co: 2.49 fm, and O: 5.803 fm) vary irregularly with atomic number and isotope and are essentially independent of d-spacing.[3] TOF neutron diffraction data were fit using the Rietveld method as implemented in the TOPAS software package (Bruker-AXS, version 6) over a d-spacing range of 2.6 Å–0.2 Å, using data from the three highest angle banks with central angles of 65° (Bank 3), 120.4° (Bank 4), and 150.1° (Bank 5). The diffraction peak shapes were primarily modeled using a pseudo-Voigt function with convolutions to model the moderator-induced asymmetrical peak shape, with a representative TOPAS input file provided as supplementary material.

III. RESULTS AND DISCUSSION

Many of the most important industrial battery cathode materials for mobile electronics and for vehicular applications are members of the α-NaFeO$_2$ structure type (Fig. 1) which belongs to space group *R-3m* and has three crystallographic sites. In the case of the prototypical Li-ion battery material, LiCoO$_2$, each chemical species in the compound is associated with a single crystallographic site, namely, the 3a Wyckoff position for Li, the 3b position for Co, and the 6c position for O. The 3b position can more broadly be considered to be a transition metal (TM) site, as reflected in newer generation cathode materials such as NMC compounds with nominal composition $Li(Ni_xMn_yCo_z)O_2$ that have a mixture of transition metals on the 3b site. While the different types of chemical species are perfectly segregated to their own crystallographic sites in the ideal structure, real materials will commonly have some combination of defects including (1) anti-site defects resulting from mixing between sites and (2) off-stoichiometry relative to the ideal composition. We generally term these defects "occupancy defects," as their presence changes the relative scattering power (an experimentally measurable quantity in diffraction experiments) of the crystallographic sites relative to their ideal values. In many cases, these occupancy defects lead to improved functionality. For example, commercial "LiCoO$_2$" cathodes used industrially have excess Li and are described by the formula $Li_{(1+x)}Co_{(1-x)}O_2$ and presumed site occupancies of $[Li][Co_{1-x}Li_x]O_2$.[4] By contrast, the compound "LiNiO$_2$" has been reported to commonly form with excess transition metal, leading to the formula $Li_{(1-x)}Ni_{(1+x)}O_2$ and presumed site occupancies of $[Li_{1-x}Ni_x][Ni_x]O_2$.[5] In the case of NMC compounds, it is generally known that there is a
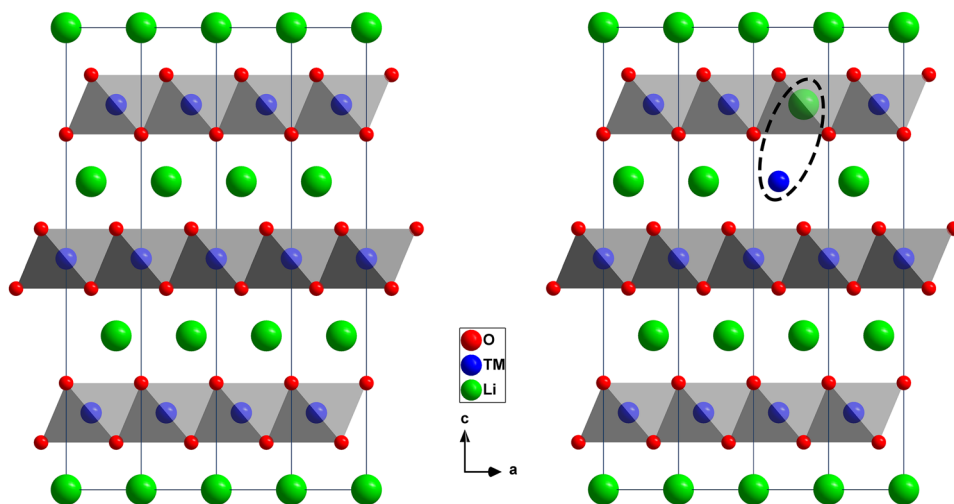
FIG. 1. Left: The ideal layered α-NaFeO$_2$ structure type of NMC compound. Within this *R-3m* symmetry structure, the transition metal atoms (TM, blue) of Ni, Co, and Mn are in octahedral coordination with oxygen atoms (red), and these octahedra (gray) share edges to form 2D planes which are separated from each other by planes of Li atoms (green). Right: Example of a paired anti-site defect of Li$_{Ni}$ and Ni$_{Li}$.

strong tendency of Ni^{2+} to participate in paired anti-site defects in which equal amounts of Ni$_{Li}$ and Li$_{Ni}$ defects are formed due to Li and Ni swapping their positions.[6] There has also been a strong recent interest in the performance of "Li-excess" compounds which derive from the compound Li$_2$MnO$_3$ which has presumed site occupancies of [Li][Ni$_{2/3}$Li$_{1/3}$]O$_2$.[7,8] The "Li-excess" compounds most strongly considered for applications are best described as a solid solution between end members of Li$_2$MnO$_3$ and Li(Ni$_x$Mn$_y$Co$_z$)O$_2$ with a lesser degree of Li excess than pure Li$_2$MnO$_3$.[9–11]

Given the large variety of defect models and the large potential influence of these defects on functionality, it is of critical importance to be able to accurately quantify these occupancy defects if structure-property relationships are to be elucidated. Modern neutron and synchrotron sources are essential for this purpose, both due to the high counting rates which can be achieved and to the wide range of data that can be collected (d_{min} of 0.5 Å or less). For the NMC compounds which will be the focus of the present work, there is limited sensitivity to the contributions of light elements in synchrotron X-ray experiments since the scattering power increases proportionally with the atomic number, Z, which is small for both Li ($Z = 3$) and O ($Z = 8$). Furthermore, the scattering power of Ni ($Z = 28$), Mn ($Z = 25$), and Co ($Z = 27$) is very similar, making the refinements generally insensitive to the relative amounts of these three transition metals in the structure. By contrast, neutron diffraction experiments are quite sensitive to the scattering from O ($b = 5.803$ fm), and while Li ($b = -1.90$ fm) remains a weak scatterer, its negative scattering length provides certain sensitivity advantages. Furthermore, the contrast between the contributions of the three types of transition metals is superb given the large differences in their scattering powers (Ni, $b = 13.3$ fm; Mn, $b = -3.73$ fm; Co, $b = 2.49$ fm). This large difference in sensitivity to all of the atomic species makes it possible to cross-validate structural refinements carried out using only neutron or only synchrotron diffraction data, as agreement between independently refined structural models will only occur if all atomic site occupancies are correctly described for the five atomic species. In this manner, it will be possible to simultaneous explore the suitability of neutron powder diffraction and synchrotron neutron

diffraction for quantifying the key occupancy defects in NMC compounds.

A. Atomic displacement parameters (ADPs)

A series of NMC samples of nominal composition Li(Ni$_x$Mn$_y$Co$_z$)O$_2$ were obtained both from collaborators and from industrial sources, with nominal compositions varying in their Ni transition metal fraction from 33% (in LiNi$_{1/3}$Mn$_{1/3}$Co$_{1/3}$O$_2$, NMC333) to 94% (in LiNi$_{0.94}$Co$_{0.06}$, NMC940006). A full list of these compounds and their abbreviations is provided in Table S1. An initial attempt to quantify defects in these compounds was carried out by assuming that (1) the nominal composition is the actual composition and (2) the only type of defect present is paired anti-site defects of Ni$_{Li}$ and Li$_{Ni}$, where the defect fraction x is defined as the fractional occupancy of defect species at both the Li (3a) and TM (3b) site. Furthermore, this refinement was carried out independently for each compound and for each type of radiation (neutron or X-ray) with no constraints on the displacement parameters between data sets, with isotropic displacement parameters used for the Li and TM sites and anisotropic displacement parameters used for the oxygen site. For any given structural refinement, all transition metals were constrained to have the same displacement parameters and it was assumed that the displacement parameter of a given atomic species did not change as a result of anti-site defect formation (e.g., the same B value used for Li$_{Li}$ and Li$_{TM}$). When anti-site defects were modeled, the same value of the cylindrical absorption corrections was applied to X-ray diffraction data assuming a packing density of 48% theoretical, the average value measured across multiple samples. Cylindrical absorption corrections for neutron diffraction data were independently refined for each bank of each sample and were generally found to be small and consistent with the values estimated based on the expected density and known absorption cross sections of the different atomic species. The values used (X-ray) or refined (neutron) for these data sets are provided in Table S2. The anti-site defect concentrations refined in this manner are plotted in Fig. 2(a) and are tabulated in Table S3, while the accompanying atomic displacement parameters from the refinements are tabulated in
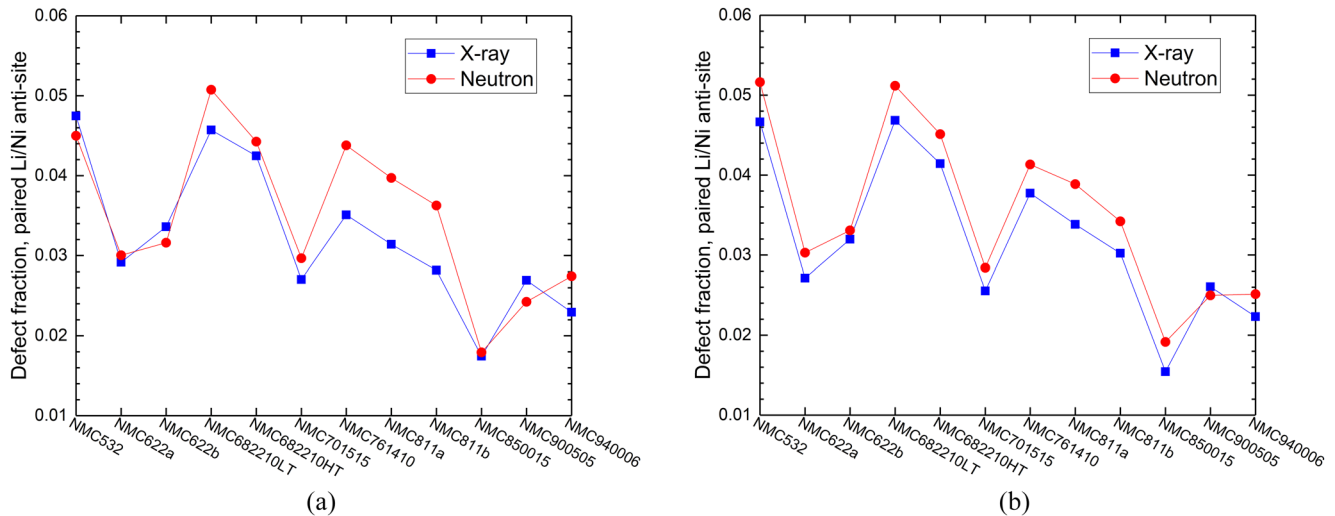
FIG. 2. Refined fraction x of paired anti-site defects of Li_{Ni} and Ni_{Li} with a general site-specific formula of $[Li_{1-x}Ni_x][TM_{1-x}Li_x]O_2$ for each NMC composition when (a) ADPs are independently refined for each data set or (b) ADPs for each crystallographic site are globally refined to a common value for all X-ray data sets and a different common value for all neutron data sets.

Table S4 and plotted in Fig. S2. Data for the NMC333 samples are omitted for reasons that will be discussed in more detail later. On the whole, there is good consistency between the paired anti-site defect fractions refined from neutron and synchrotron data, though the mean difference (0.40% absolute) and the maximum difference (0.87% absolute) between the two data sets are both undesirably large relative to the amount of defects refined for these samples (1.5%–5%).

If greater precision is to be achieved, it is important to understand the origin of the discrepancies between the neutron and X-ray results. One likely source is uncertainty in the atomic displacement parameters (ADPs), which were refined in the form of isotropic B-values. It is often underappreciated

that the total scattering power at an atomic site (and therefore the refined site occupancy) is strongly dependent on the displacement parameter associated with the site, as illustrated in Fig. 3(a). If an atomic site which has a B-value of 0.5 Å is instead treated as having a B-value of 1.0 Å, the calculated scattering power from that site can be increased by more than 25% over many scattering vectors (Q) sampled during the experiment when the calculated scattering powers are corrected for the loss in coherent scattering intensity due to atomic displacements from their ideal lattice positions. In order to accurately determine site scattering occupancies, it is therefore critically important to ensure that refinements are carried out with correct ADP values (which are known to be very challenging to
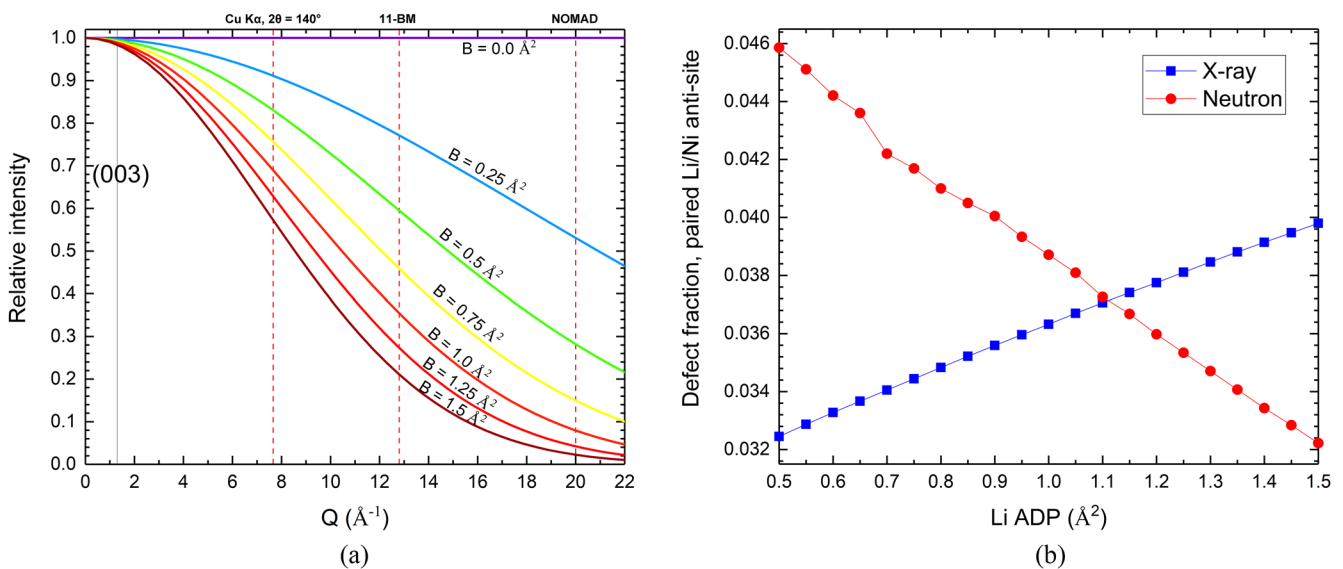

FIG. 3. (a) Intensity reduction due to isotropic atomic displacements plotted as a function of Q ($=2\pi/d$) for selected B-values ranging from 0 to 1.5 Å^2. Positions are indicated for the Q_{max} values for a typical Cu Kα laboratory diffractometer, for standard data from the 11-BM diffractometer at the APS synchrotron, and for standard data from the NOMAD neutron diffraction beamline at the SNS. (b) Influence of the Li B-value on the refined concentration x of paired anti-site defects with a site-specific formula of $[Li_{1-x}Ni_x][TM_{1-x}Li_x]O_2$ in the compound NMC811a with a nominal stoichiometry of $Li(Ni_{0.8}Mn_{0.1}Co_{0.1})O_2$.

accurately determine from powder diffraction data). This can be clearly seen in the variation in the refined anti-site defect fraction that occurs when the Li *B*-value is varied between 0.5 and 1.5, while the other *B*-values are held constant [Fig. 3(b)], resulting in defect fractions ranging from 3.2% to 4.0% (absolute) in synchrotron X-ray refinements and from 4.6% to 3.2% (absolute) in neutron refinements. This represents a typical range of Li *B*-values that are reported in the literature for powder diffraction studies on this class of Li-ion battery systems and suggests that immense errors of 0.6%–1.4% (absolute) can easily occur if correct *B*-values are not used in Rietveld refinements. Similar plots for the ADPs for the transition metals and oxygens are provided in Fig. S3.

There are three primary considerations that are needed to properly determine *B*-values. The first is the application of an accurate absorption correction since absorption coefficients and displacement parameters have a very similar functional form and can therefore be very strongly correlated. For synchrotron X-ray diffraction data, this was accomplished by experimentally determining the average sample packing fraction (based on the sample mass, sample length, and capillary diameter) and applying a cylindrical absorption correction calculated for the X-ray wavelength using this information. All X-ray samples were assumed to have the same packing density in order to avoid the undesirable scatter due to the experimental difficulty of precisely measuring densities. For the time-of-flight neutron diffraction data, it is impractical to directly calculate the absorption required absorption correction since (1) many detectors are present outside of the normal plane of scattering so the assumptions made during the calculation of conventional cylindrical absorption corrections are not strictly valid as path lengths through the sample are underestimated and (2) the wavelength dependence of the absorption coefficient cannot be rigorously treated in data sets after merging since the count rates recorded at any given *d*-spacing are the summed contributions from neutrons of different wavelengths. However, one specific advantage of data collection on the high-flux NOMAD instrument is that the sample radius utilized during data collection can be small ($R \sim 1.5$ mm), helping keep the sample absorption coefficients across the entire series of NMC low (calculated $\mu R \leq 0.1$ for 1 Å neutron wavelength based on measured can diameter and sample packing density). For this reason, it was deemed appropriate to empirically refine the μR product in a conventional Lobanov-type cylindrical absorption correction. The values refined in this manner (Table S2) are consistent with values estimated based on sample composition and expected packing fractions.

The second consideration is that data must be collected over a wide range of *Q* (or equivalently, *d*) in order to be able to accurately determine *B*-values since there are only slight differences in the functional form for slightly different B-values. One consequence of this is that it is generally not possible to accurately determine *B*-values from Cu $K\alpha$ laboratory diffraction data, which only extends from $Q \sim 1$ Å^{-1} (first NMC diffraction peak) to $Q \sim 8$ Å^{-1}. By contrast, high resolution 11-BM is routinely collected out to $Q \sim 13$ Å^{-1}, and NOMAD data for these samples are even more favorable as data out to $Q \sim 20$ Å^{-1} can easily be obtained even when using readily accessible sample masses (~100 mg) and data collection

times (~1 h). The range of relative intensities spanned by each of these three instruments is marked in Fig. 3(a). The third and final consideration is that a much more accurate measure of the displacement parameters can generally be obtained if the values for each atomic site are globally constrained to be the same across all samples in the series, as implemented through a parametric refinement. This was initially done for the neutron samples which have the three key advantages over the synchrotron data: a wider *Q* range, more favorable atomic form factors (minimal loss of intensity at higher *Q*), and far lower absorption of the incident radiation ($\mu R \sim 0.075$ *vs.* $\mu R \sim 0.5$, details in Table S2). After the neutron ADPs were determined through a global refinement, the X-ray ADPs were fixed to the globally refined neutron values (Li, $B = 0.943$ Å^2; TM, $B = 0.295$ Å^2; O, $u_{11} = 0.0103$ Å; and $u_{33} = 0.0077$ Å) as identical samples were used in both the synchrotron and neutron data collection. The implementation of globally parameterized ADPs taken only from neutron refinements produced a stunning improvement in the similarity of the defect fractions obtained through independent refinements using synchrotron and neutron data [Fig. 2(b)], with the values provided in Table S3 and accompanying ADPs provided in Table S4. While the mean difference between the synchrotron and neutron defect fractions has slightly decreased from 0.40% to 0.34% (absolute), the errors are now clearly seen to be systematic rather than random. If an optimal linear offset of 0.32% absolute is incorporated, the mean difference between the X-ray and neutron data is greatly reduced to 0.12% (absolute). Further work is required to determine the origin of this offset, and in Sec. III B, we develop the tools for doing so.

B. Diffraction parameter space for NMC compounds

For the diffraction pattern of a crystalline solid that is well described by the concept of a periodic unit cell, all of the information about the location and quantities of atomic species within a unit cell is fully encoded in the diffraction peak intensities, I_{hkl}, which are derived from the overall structure factors for the reflections, F_{hkl}. Once the positions of the atomic sites are known, the only remaining parameters that influence peak intensities are the scattering power at each atomic site, which can be determined through the relationship $f_{xyz} = \sum_i c_i f_i$, where the scattering power of a site with fractional coordinates of (x, y, z) is the sum of the product of the atomic form factors, f_i, and the fractional occupancy, c_i, for each of the *i* species residing at the site. Rather than working individually with each atomic site, it is easier to group together the sets of *m* indistinguishable atomic sites that are related to each other by the symmetry of the cell, and to work with them as a single crystallographic site of multiplicity *m*. While for an arbitrary *hkl* reflection, the net scattering power of the *m* atoms comprising a single crystallographic site with multiplicity *m* is typically less than *m* times the scattering power of a single one of these atoms due to the fact that the scattering from the component atoms is not perfectly in phase, if we consider the hypothetical F_{000} reflection which occurs at $2\theta = 0$, it will always be true that the scattering power of *m* atoms is equal to *m* times the scattering power of a single atom. We therefore define a specific zero-angle crystallographic site scattering power of

$f_n^* = m \sum_i c_i f_i$, where the total zero-angle scattering associated with the nth crystallographic site is equal to the product of the site multiplicity m and the scattering power associated with each site. These n crystallographic site scattering powers necessarily obey the sum rule $\sum_n f_n^* = F_{000}$.

These f^* values provide an important conceptual means of understanding the influence of site occupancy on diffraction peak intensities. In a perfectly coherent lattice without atomic displacements, the structure factor associated with any reflection can be decomposed into a linear sum of the crystallographic site scattering factors f^* (which are the same for every reflection) multiplied by a phase factor ω with a value ranging from $+1$ to -1 (where ω is individually determined for each reflection based on the phase relationships between the m contributing atomic sites with respect to the specific scattering vector of the reflection, making ω independent of the site occupancies), $F_{hkl} = \sum_n \omega_n f_n^*$. In this manner, it can be seen that for a structure with n crystallographic sites, the observed pattern of peak intensities depends only on the effects of n site scattering powers. However, it should be noted that the overall scale factor of a diffraction pattern is typically not measured but is instead treated as a refined parameter. As a consequence, refinements are then sensitive only to the relative and not the absolute values of the n scattering powers. When this is the case, then the n crystallographic site scattering powers cannot be independently probed, and instead represent $(n-1)$ independent parameters. These $(n-1)$ parameters represent the total amount of information about site occupancies that can be extracted from Rietveld refinement of a single diffraction pattern in the absence of an absolute reference. One well-known consequence is that it is impossible to simultaneously refine the occupancy of all atomic sites, as proportionally scaling the occupancy of all sites will result in a diffraction pattern that is indistinguishable from the original.

In the case of standard α-NaFeO$_2$-type NMC compounds, there are 3 types of crystallographic sites (Li, 3a; TM, 3b; O, 6c), so the entire parameter space associated with the site occupancies of any NMC compound sampled through a single diffraction measurement must be 2-dimensional (2D) in nature. In other words, every possible diffraction pattern that could be generated by varying site occupancies can be specified using coordinates within this 2-dimensional parameter space. An efficient and effective manner of representing this entire parameter space would greatly facilitate the interpretation and analysis of powder diffraction data, though we are not aware of any prior generally used conventions for doing this. However, we note that ternary phase diagrams are a widely utilized tool for representing the 2D parameter space associated with the composition of chemical compounds with 3 components. In ternary phase diagrams, one of the 3 potential degrees of freedom is lost due to the fact that relative fractions (and not absolute amounts) of the 3 chemical constituents are being plotted, behavior which is conceptually and mathematically analogous to the behavior of site scattering powers in Rietveld refinements.

It is therefore suggested that triangular f^* diagrams can be a similarly effective tool for understanding the 2D parameter space associated with occupancy defects in ternary (or higher) compounds with three crystallographic sites. The three axes in f^* diagrams are chosen to display the fractional contribution of the scattering power from each crystallographic site relative to the total scattering power of the compound (F_{000}) at $2\theta = 0$. For any α-NaFeO$_2$-type NMC compound, the coordinates along these axes can be directly calculated from the crystallographic site compositions and from the relevant atomic form factors. Each ideal, defect-free, NMC crystal structure corresponds to a single position within the triangular 2D parameter space of a f^* diagram. The ideal positions in an X-ray f^* diagram for every NMC compound studied in this work are shown in Fig. 4(a). The coordinates of all of the compounds are clustered close together since the differences in the X-ray scattering factors for Ni, Mn, and Co are small. However, a larger separation is found between the same compounds in their neutron f^* diagram [Fig. 4(b)] due to the very
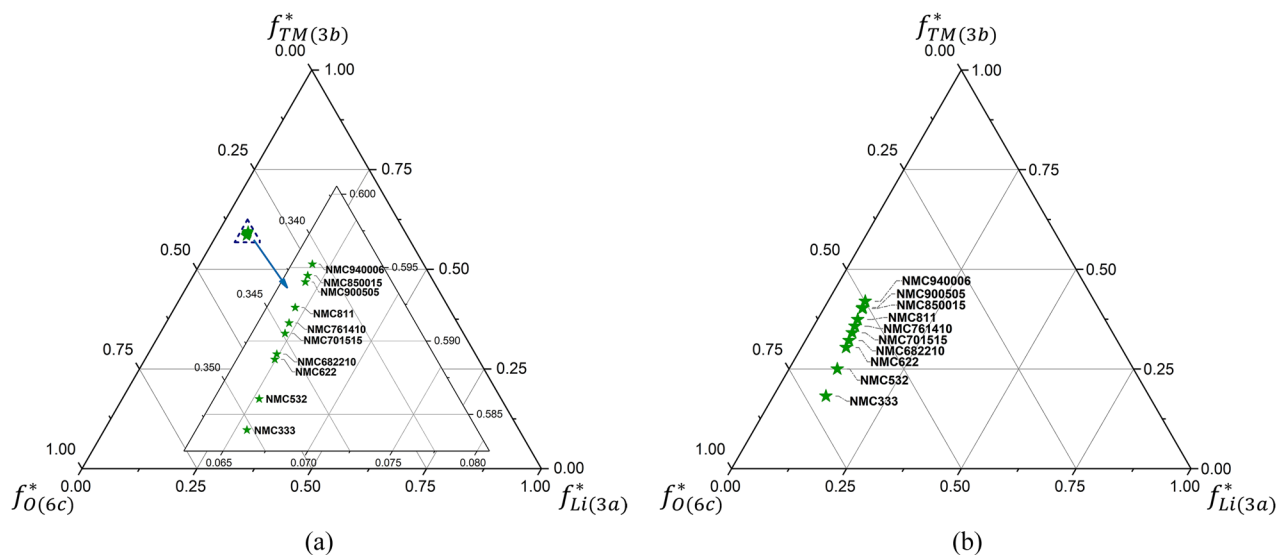

FIG. 4. Overall f^* diagram for (a) X-rays and (b) neutron data for all NMC compounds studied in this work (Table S1), shown both at full scale and with a zoom into the region where compounds are clustered in the X-ray diagram.

large neutron scattering contrast between these three transition metals.

Although the f^* coordinates of any ideal NMC compound are necessarily fixed, any occupancy defects present in the compound will change the relative scattering power of the three crystallographic sites and will necessarily shift the coordinates of the compound in this parameter space. This is illustrated for the specific example of the X-ray f^* diagram for the compound Li(Ni$_{1/3}$Mn$_{1/3}$Co$_{1/3}$)O$_2$ in Fig. 5(a). Each type of occupancy defect is represented by a different vector moving away from the coordinates of the ideal composition, and the length of the vector corresponds to the shift in parameter space when the fraction of the occupancy defect is $x = 0.10$. The length of the vector therefore provides a first estimate of the sensitivity of diffraction data to different types of occupancy defects. Furthermore, the more collinear that the vectors associated with different types of defects are, the harder it should be to use a single experimental diffraction pattern to discriminate between these two types of defects. When vectors are exactly collinear, both defect types will sample exactly the same line across of parameter space and it will be virtually impossible to use a single diffraction pattern to distinguish between these two types of defects (as the only opportunity to distinguish between models will come from differences in the Q-dependence of atomic form factors, which are typically very small). This is necessarily the case for two defects that both modify the scattering power of a single site in the same manner, for example, the replacement of Li$_{Li}$ with Co$_{Li}$ or with Ni$_{Li}$.

In addition to illustrating the difficulty distinguishing between certain types of single defects, the f^* diagram visually demonstrates the challenges in resolving occupancy defects in systems where more than one type of occupancy defect is present. Since the f^* diagram inherently represents all possible diffraction patterns that can be obtained for a given structure type by arbitrarily varying crystallographic site occupancies, the coordinates in the f^* diagram of the true structural

model for a system will represent a global minimum in the R_{wp} that can be obtained through refinement of site occupancies (assuming that it is not possible to distinguish between the angular dependence of different atomic form factors, an assumption which is weakly violated for X-ray data and is not meaningfully violated for neutron data). Although the global minimum corresponds to a single position within the f^* diagram, the coordinates of this global minimum can be specified through using a linear combination of the vectors that shifts away from the ideal composition for ***any*** two occupancy defect models. An example of this is shown in Fig. 6(a) for refinements against the experimental synchrotron X-ray diffraction data collected for Li(Ni$_{1/3}$Mn$_{1/3}$Co$_{1/3}$)O$_2$ using the optimal refinement parameters that will be discussed in Sec. III C. This compound clearly has more than one type of occupancy defect, as none of the single defect models tested (red triangles) attain the R_{wp} of the global best fit, though the paired anti-site defects of Li$_{Ni}$ and Ni$_{Li}$ at a fraction of 0.0240 come closest (8.852 vs. 8.637). When double defect models are tested (blue circles), it can be seen that the f^* diagram coordinates (Table S5) determined from a variety of different double defect models cluster together very closely and are indistinguishably close to a global minimum in R_{wp} (8.637–8.642), despite the very different types and concentrations of defects refined in these different models (Table I). For example, the global minimum can be reached using 1.79% paired anti-sites and 4.85% Li excess ($R_{wp} = 8.637$), using 2.21% paired anti-sites and -4.27% oxygen vacancies ($R_{wp} = 8.641$), or even using 25.8% Li excess and 18.7% oxygen vacancies ($R_{wp} = 8.630$). From these data, it is clear that the correct concentration of any one occupancy defect can only be obtained when all other occupancy defects are properly treated (included or excluded from refinement)—incorrect choices lead to wildly different refined concentrations, as can be seen for the data in Table I. Furthermore, the inclusion of defects such as oxygen vacancies that are not actually present in the system will substantially
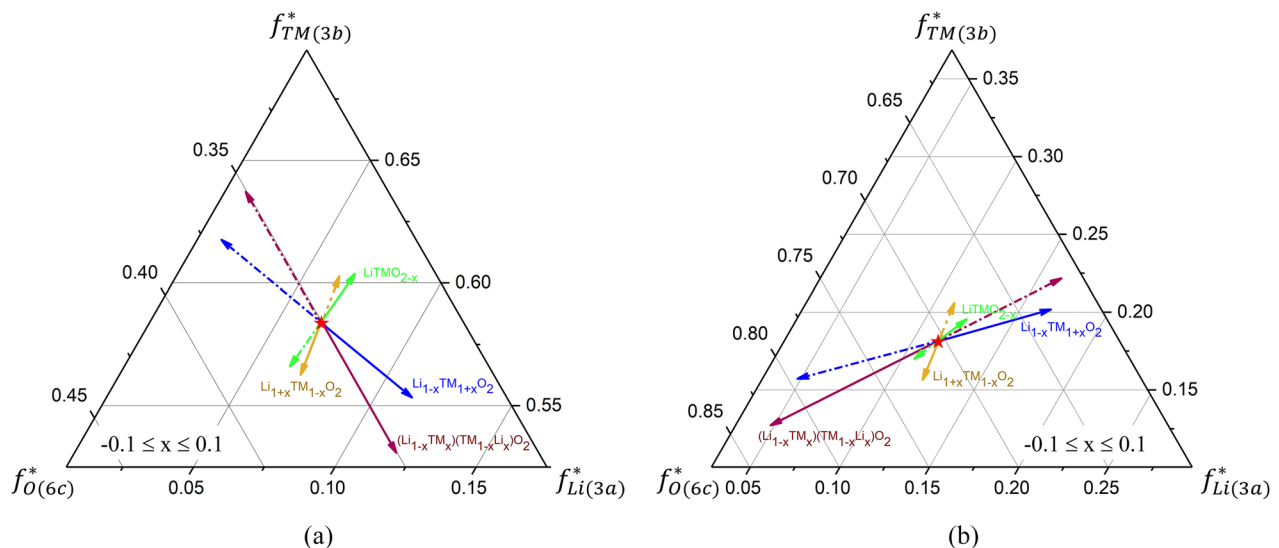

FIG. 5. Comparison of f^* diagrams for (a) X-ray and (b) neutron data for Li(Ni$_{1/3}$Mn$_{1/3}$Co$_{1/3}$)O$_2$, denoted as NMC333. Occupancy defects are shown as vectors pointing to the coordinates that result from a value of $x = +0.1$ (solid) and $x = -0.1$ (dashed-dotted) for the specific defect models of (1) paired anti-site defects of Li$_{Ni}$ and Ni$_{Li}$ (maroon), [Li$_{1-x}$TM$_x$][TM$_{1-x}$Li$_x$]O$_2$, where the only TM to swap sites is Ni; (2) Li excess (gold), [Li][TM$_{1-x}$Li$_x$]O$_2$; (3) transition metal excess (blue), [Li$_{1-x}$TM$_x$][TM]O$_2$; (4) oxygen vacancies (green), LiTMO$_{2-x}$.
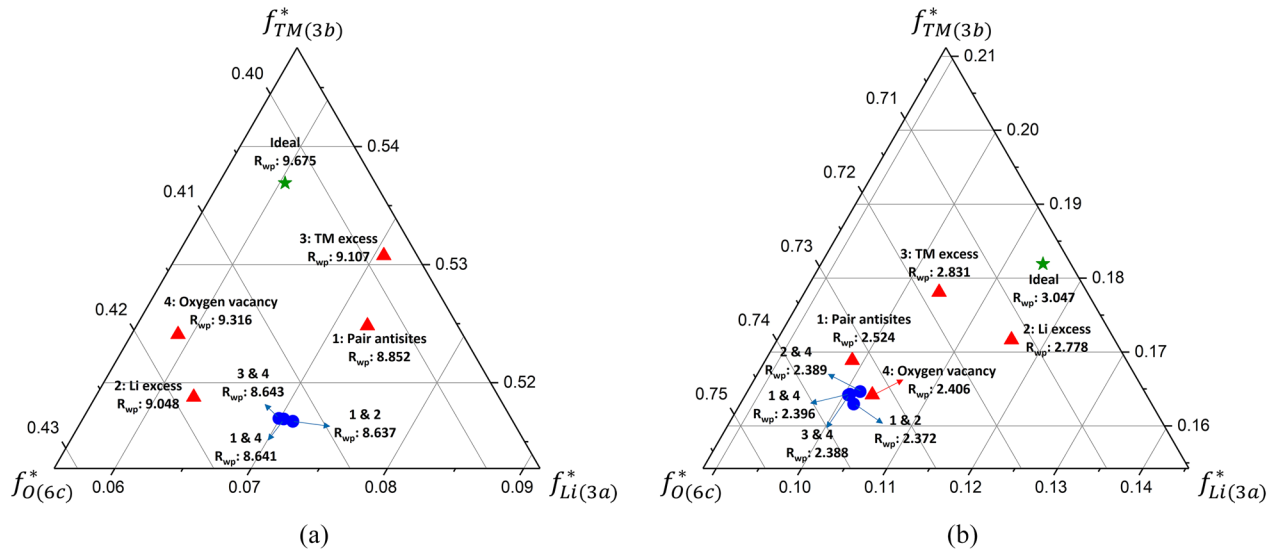
FIG. 6. Experimentally determined (by Rietveld refinement) coordinates for NMC333a within f^* diagrams for various single defect models (red triangles) and double defect models (blue circles) relative to those calculated for the ideal defect-free structure (green stars), labeled with refinement R_{wp} values for each model for (a) X-ray and (b) neutron experiments. Refined defect concentrations for these fits are given in Table I. Results were obtained using fixed B-values (from global refinements against neutron data) and final optimal X-ray atomic form factors, as will be described later.

improve the refinement R_{wp}, making it easy to reach erroneous conclusions about the underlying structural model.

The subtle differences in the fit R_{wp} and in the slightly different f^* diagram coordinates of the different double defect refinements are primarily due to the slight differences in the angular dependence of the atomic form factors. This is most clearly seen when the results for a double defect model that varies the amounts of the lightest atoms (Li excess and oxygen vacancies) are compared to the other double defect models (Fig. S4), as it can be seen that this light atom model is substantially displaced from the cluster of other double defect models. These systematic errors go away when the same double defect models are tested against the neutron diffraction data for the same compound [Fig. 6(b)] since the neutron atomic form factors are all very close to being angle-independent as a result of atomic nuclei being much smaller (diameter $\leq 2 \times 10^{-14}$ m) than the range of periodicities sampled in diffraction experiments ($d_{min} \geq 10^{-11}$ m), though the neutron points are still somewhat less closely clustered likely due to the substantially reduced counting statistics relative to the synchrotron data.

Some powerful aspects of f^* diagrams are highlighted from this analysis. First, it is easy to determine where in the entire diffraction parameter space the global minimum is located, even if the physically correct defect model is unknown. This goes a long way to resolving a longstanding general question in Rietveld refinements—when is the refinement good enough? Second, a consequence of this is that by comparison to the global minimum coordinates, it can readily be determined whether a system contains only a single type of occupancy defect or multiple types of occupancy defects. In contrast to the NMC333a compound shown in Fig. 6, most other NMC compounds only exhibit a single type of occupancy defect. This is illustrated in Fig. 7 for a representative compound of NMC682210HT. From both the X-ray and neutron f^* diagrams, it is clear that the single defect type of paired anti-site defect of Li_{Ni} and Ni_{Li} (red vector) produces a fit indistinguishable from a global minimum fit constructed from a double defect model (blue vector). The refined concentrations (Table S6) and f^* diagram coordinates (Table S7) associated with these fits are provided as supplementary material.

TABLE I. Defect fractions and refinement R_{wp} values for different single and double-defect NMC333a structural models.

|	X-ray				Neutron				
Defect model	R_{wp}	Anti-site	Li excess	TM excess	O vacancy	R_{wp}	Anti-site	Li excess	TM excess	O vacancy
Ideal	9.675	0	0	0	0	3.047	0	0	0	0
1. Pair anti-site	8.852	0.0240	0	0	0	2.524	0.0268	0	0	0
2. Li excess	9.048	0	0.0791	0	0	2.778	0	0.0419	0	0
3. TM excess	9.107	0	0	0.0220	0	2.831	0	0	0.0167	0
4. O vacancy	9.316	0	0	0	−0.0608	2.406	0	0	0	−0.1533
1 and 2	8.637	0.0179	0.0485	0	0	2.372	0.0232	0.0300	0	0
1 and 4	8.641	0.0221	0	0	−0.0427	2.396	0.0106	0	0	−0.1073
2 and 4	8.630	0	0.2578	0	0.1868	2.389	0	−0.0115	0	−0.1739
3 and 4	8.643	0	0	0.0241	−0.0642	2.388	0	0	0.0065	−0.1400
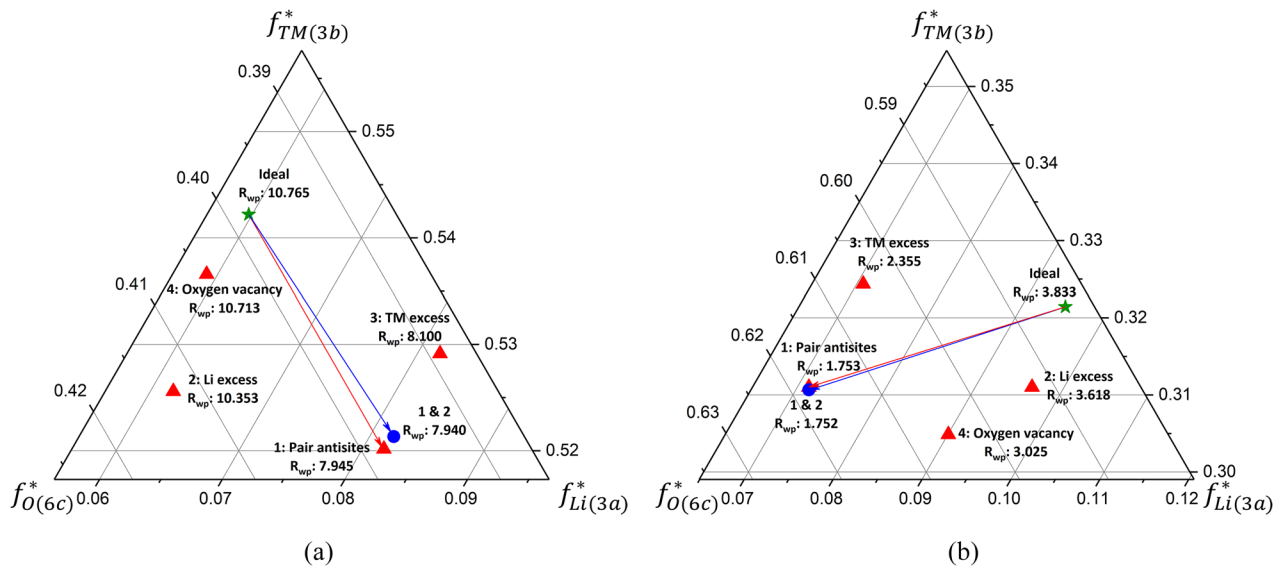
FIG. 7. The dominant defect model in NMC682210HT (shown) and most other NMC compounds (not shown) is paired anti-site defects of Li_{Ni} and Ni_{Li} as seen by the close proximity of this single defect model (red vector) to the global minimum (blue vector) determined using a double-defect fit for (a) X-ray and (b) neutron experiments. Furthermore, the concentration of this defect obtained through Rietveld refinement (using global neutron ADPs and optimal X-ray atomic form factors) is very similar when using X-ray (4.43%) or neutron (4.52%) data. Concentrations of defects refined using different models plotted in this figure are given in Table S6 while corresponding f^* diagram coordinates are given in Table S7.

While the present analysis is concerned with compounds with three crystallographic sites, it is straightforward to extend this method to compounds with more atomic sites in direct analogy with higher order phase diagrams. If the defects of interest affect two or fewer sites, a simplified f^* diagram analogous to a 2D pseudo-ternary phase diagram can be used to capture the cross section of the scattering power parameter space for which the occupancy is unknown and needs to be resolved. The scattering power from all other crystallographic sites for which the occupancy is certain can be combined together and treated as a single corner of this type of simplified f^* diagram. Finally, a third powerful aspect of the f^* diagram is that if there is a problem with the atomic form factors, this will cause a clear systematic shift that can be observed and corrected, as will be discussed in detail in Sec. III D.

Although only two site occupancy parameters can be extracted from refinement against a single diffraction pattern, twice as many occupancy parameters can be resolved when refining against two diffraction patterns whose intensities are determined by distinctly different types of atomic form factors, as is the case for complementary X-ray and neutron diffraction data. The independence of parameters can be seen by comparing Figs. 5(a) and 5(b), in which it can be seen that for a given type of defect model both the length and orientation of vectors differ between the X-ray and neutron f^* diagrams. The vector length provides an estimate of the sensitivity of a specific measurement technique to the defect concentration. From this f^* diagram construction, it can be seen that while it is impossible to distinguish between collinear single defect vectors (such as those corresponding to Ni_{Li} and Co_{Li} defects) using a single type of radiation, these defects can be generally distinguished using the combination of X-ray and neutron diffraction data since only one type of defect vector will correctly describe the length of the observed vector shift away from the ideal

composition simultaneously in both the X-ray and neutron parameter spaces. For the present NMC samples, the available diffraction data allow a total of 4 parameters associated with occupancy defects to be determined and it can therefore be said with great confidence that the dominant defect model is paired anti-site defects of Ni_{Li} and Li_{Ni} as this single defect model points to the global minimum in both X-ray and neutron f^* diagrams for the majority of compounds, and the remainder of compounds can be satisfactorily modeled using just two types of occupancy defects.

C. Systematic trends in x-ray and in neutron f^* diagrams

Just as f^* diagrams can be used to clarify the nature of occupancy defects in a single compound, the comparison of a related series of compounds plotted on a single f^* diagram constructed from either X-ray or neutron and X-ray data can make clear systematic trends across a class of compounds. The present data on NMC compounds offer the opportunity to use an extensive series of related compounds with the constraint of a well-established dominant defect model type to look for minor secondary effects that could not confidently be identified when a single compound is studied. As was highlighted in Fig. 7, there are typically small differences between refinements of neutron powder diffraction data constrained to have a single defect type of paired anti-site Ni_{Li} and Li_{Ni} defects and unconstrained double-defect refinements. However, for the same samples, this was not the case for the corresponding synchrotron X-ray diffraction data. When the results for refinements against synchrotron data for all 14 different NMC samples studied in this work obtained using X-ray atomic form factors for neutral atoms were plotted together on a single f^* diagram [Fig. 8(a)], it can be seen that the anti-site
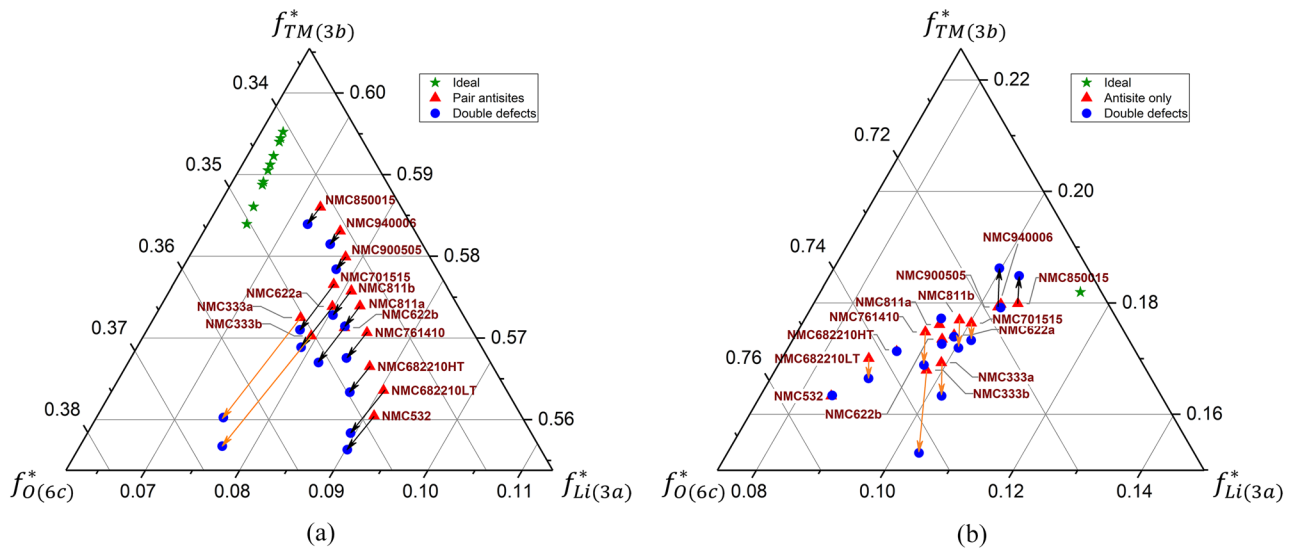
FIG. 8. Systematic f^* diagram trends for all 14 NMC samples for (a) X-ray and (b) neutron data. Green stars indicate ideal coordinates, red triangles indicate single defect model (Ni$_{Li}$ and Li$_{Ni}$) positions, blue circles indicate global double defect minima, and vectors indicate the difference between the single and double defect coordinates (for refinements using global neutron ADPs and optimal X-ray atomic form factors). All neutron data have been offset so that their ideal coordinates match those of NMC333.

defect models never coincide with the global minima established through double-defect refinements. The largest differences (orange arrows) were seen for two samples of NMC333, which were through their individual f^* diagram plots found to both contain substantial amounts of two different types of occupancy defects. Intriguingly, it was observed that the vector displacement (black arrows) between the coordinates of the single-defect refinements (red triangles) and the global double-defect refinements (blue circles) was very similar in the direction and magnitude for all of the remaining samples. Furthermore, when extended across the full range of the f^* diagram, these vectors were observed to point directly at the corner associated with the oxygen site scattering power. This result strongly suggests the existence of a correctable systematic error associated with the use of neutral oxygen form factors. The process for identifying an optimal choice of X-ray atomic form factors will be discussed in Sec. III D.

Although there is no evidence of systematic errors in the neutron refinement results when studied in the context of a f^* diagram, this diagram does offer insights into the nature of secondary defects in some NMC samples. In order to compare NMC defects in the neutron f^* diagram, the three data points for each compound have been translated by a common vector so that the coordinates of each ideal NMC composition overlap those of the compound Li(Ni$_{1/3}$Mn$_{1/3}$Co$_{1/3}$)O$_2$ with the single green star shown in Fig. 8(b) placed at these coordinates, thereby allowing all 14 samples to be simultaneously compared at a suitably high zoom. For about half of the compounds, the single defect model (red triangle) and the double defect global minimum (blue circle) are observed to coincide, indicating that the only detectable defect is pairs of Ni$_{Li}$ and Li$_{Ni}$. For the remainder of the compounds, a second defect appears to be present, though with a smaller influence on the overall refinement as can be judged by the reduction in the refinement R_{wp} when including the second defect in structural models which is typically about 1/10 of that achieved through

the inclusion of paired anti-site defects of Ni$_{Li}$ and Li$_{Ni}$. The nature of this secondary defect can be ascertained from the vector relationship between the coordinates of the paired anti-site defect only and the global double defect minimum fit results. In all cases, this vector points either toward (black arrows) or away (orange arrows) from the general direction of the transition metal corner at the top of the f^* diagram. This behavior will occur if the secondary defect affects the scattering power at the transition metal site only, either increasing it (black arrows) or decreasing it (orange arrows).

There are two likely physical origins of this observed behavior. The first is overall cation non-stoichiometry with excess Li described by the formula [Li][TM$_{1-x}$Li$_x$]O$_2$. Any excess Li in compounds will reside at the TM site, thus substituting TM$_{TM}$ with Li$_{TM}$ and thereby reducing the scattering power at the TM site. The second likely origin is non-stoichiometry in the ratio of transition metals, where the values of x, y, and z differ between the nominal and actual composition of Li(Ni$_x$Mn$_y$Co$_z$)O$_2$. This could result in the transition metal scattering power being either slightly higher (Ni excess) or slightly lower (Mn excess or Co excess) than the ideal value, as judged by the relationship of the scattering length of each element to the average scattering length of the site as a whole. Since the neutron scattering lengths of the transition metals are extremely different, even slight differences can provide noticeable shifts, in direct contrast to the X-ray results which are for the most part insensitive to variations in the relative amounts of the three transition metals. It is likely that both types of non-stoichiometries are present for the NMC samples studied in this work. The two NMC333 samples studied in this work both appear to have significant Li excess, as will be described in more detail elsewhere. It has been previously reported that nominal LiNiO$_2$ often has a true composition with excess Ni that is better described as Li$_{1-x}$Ni$_{1+x}$O$_2$.[5,12,13] This is consistent with the excess scattering power observed at the TM site for the very Ni-rich samples of Li(Ni$_{0.90}$Mn$_{0.05}$Co$_{0.05}$)O$_2$

and $Li(Ni_{0.85}Co_{0.15})O_2$. Some compounds with a small deficiency of neutron scattering power at the TM site such as $Li(Ni_{0.70}Mn_{0.15}Co_{0.15})O_2$ may either have a small amount of Li excess or a small amount of Mn or Co excess, though it is difficult to unambiguously resolve which given the small influence that this secondary defect has on the overall R_{wp} of the refinement, and the small changes in the transition metal composition relative to the nominal stoichiometry (differences in x, y, and z are likely on the order of 0.01 absolute).

D. Optimal x-ray atomic form factors

Theoretical X-ray atomic form factors are for the most part calculated based on the behavior of isolated gas phase atoms,[14] and their applicability to molecular or solid state compounds is for the most part accepted based on faith, given the difficulty of accurately experimentally validating atomic form factors, especially with regard to their use for complex multi-element compounds. In the past, the unary compounds have predominantly been used for the experimental determination of the values of atomic form factors at specific scattering angles with the goal of validating the theoretically calculated atomic form factors from which the complete angular dependence can be readily extracted.[15–20] There is not a generally accepted rationale for deciding whether to use neutral (e.g., Li, Co, O) or ionic atomic form factors (Li^+, Co^{3+}, O^{2-}) for NMC compounds. Recently, there was a pioneering effort to determine which combination of neutral and ionic form factors is most appropriate for structural refinements for the important NCA battery compound, $Li(Ni_{0.85}Co_{0.10}Al_{0.05})O_2$ through comparative and co-refinements of high quality X-ray and neutron powder diffraction data.[21] While the sensitivity of the NCA refinements to different modeling choices was effectively addressed, the final choice about modeling parameters was done in the absence of direct knowledge of defect type and concentration, with some weakly tested assumptions about atomic displacement parameters, and with no correction for sample absorption in either the X-ray or the neutron diffraction data—something that is expected to introduce a systematic bias between the X-ray and neutron results that will affect conclusions about X-ray form factors. The combination of the new f^* diagram methods described here and the combination of both synchrotron and neutron diffraction data of high quality collected in this work for a related series of compounds offer the opportunity to more generally and more robustly determine the optimal choice of form factors for modeling layered battery cathodes.

In order to improve upon the use of neutral X-ray atomic form factors (which were found to give rise to systematic errors in the refined defect concentrations of NMC samples in Sec. III C), neutron diffraction data were used as a reference to assess the validity of different models for the X-ray atomic form factors since there is negligible uncertainty in the theoretical nuclear form factors. In order to evaluate the ability of different X-ray atomic form factor choices to correct for systematic errors, two different approaches were utilized to assess the results for refinements against the synchrotron data only. During this process, Rietveld refinements were carried out using the optimal methods determined in the first

section, with atomic displacement parameters fixed to values obtained from global refinements against all neutron diffraction data (though with the global refinement excluding samples observed through f^* diagrams to have a substantial amount of a second type of occupancy defect). The first assessment approach was monitoring the magnitude of the displacement between the anti-site only minimum and the double-defect global minimum in X-ray f^* diagrams, as this should be minimized with optimal form factor choices. The second assessment approach was following the concentration of the second defect refined during double-defect refinements together with paired anti-site defects, as the second defect concentration should go to zero for many samples when the X-ray atomic form factors are correct given the robustness with which the single-defect model was established using neutron diffraction data. This is especially true since one of the most likely secondary defects inferred from the neutron f* diagrams, transition metal non-stoichiometry, will have a negligible effect on X-ray refinements due to the small differences in the X-ray atomic form factors of Ni, Co, and Mn.

A comparison of the data obtained using these two approaches for the starting point (neutral atoms, left) and for the final modeling choice (neutral Li and TMs, ionic O^{2-}, right) for X-ray diffraction data is presented in Fig. 9, with additional plots of refined defect concentrations obtained through the second approach provided in Fig. S5. To facilitate comparisons, the data for each sample in Fig. 9 have been given a translational offset so that the coordinates of the ideal composition match those of the compound NMC333; corresponding plots without the offset are provided in Fig. S6. With neutral atomic form factors, the offset between the anti-site only and global models for the X-ray data corresponds to a shift of about 0.005 of the total scattering power of the compound in the oxygen direction. Furthermore, systematic errors are also seen in double-defect refinements where the refined fraction of the second defect type used in the double defect model of excess Li is on average about 0.02. When the atomic form factor for oxygen is changed from the neutral one that of ionic O^{2-}, both of these issues are resolved. There is no longer an observable systematic offset between the anti-site only and global minimum positions in the X-ray f^* diagram, and the concentration of excess Li typically refines to values in the range of +0.01 to −0.01, with the average value not obviously differing from zero. Other choices of X-ray atomic form factors generally gave worse agreement, as is shown in Fig. S5. If only the transition metals are treated using ionic form factors, the improvement in the refinement is about half as much, with an average amount of refined excess Li of about 0.01. When all atomic species are treated using their ionic form factors (Li^+, Ni^{2+} and/or Ni^{3+}, Co^{3+}, Mn^{4+}), the correction is overdone, and all NMC refinements report a negative Li excess with an average value of about −0.01 that is clearly aphysical as it corresponds to 1.01 transition metals occupying the transition metal site. The choice of Li^+ form factor had a negligible impact on the refinement due to both the small fractional contribution of Li to the overall refinement and the limited number of diffraction peaks (one) that fall in the very limited range Q-range over which the differences in the Li^+ and Li atomic form factors (Fig. S7) are potentially resolvable.
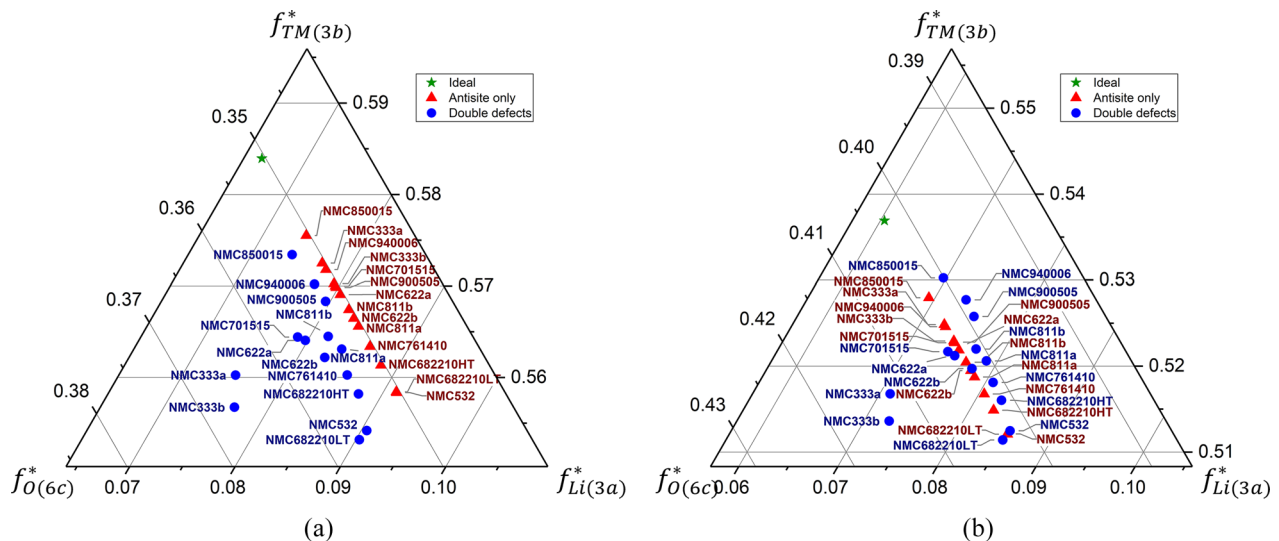
FIG. 9. Comparison of offsets between normalized X-ray f^* diagram coordinates (in which all ideal coordinates were shifted to match those of the NMC333 sample) obtained from refinements using (a) neutral atomic form factors and (b) ionic form factor for O^{2-} and neutral form factors for all other species.

The difference in the refined anti-site defect concentrations using Li^+ and Li form factors is also negligible (Fig. S8). The final modeling was therefore chosen to be carried out with the neutral Li atomic form factor due to considerations of both simplicity and of consistency with the treatment of the other cationic species.

Furthermore, when the absolute value of the paired anti-site defect fractions refined from the synchrotron X-ray data using the optimal form factors (ionic O^{2-} form factors and neutral form factors for all other species) is compared to those obtained from neutron refinements, the agreement is exceptional (Fig. 10). The offsets in the refined X-ray and neutron anti-site defect concentrations previously observed when using neutral X-ray atomic form factors (Fig. 2) are eliminated. The mean difference between the anti-site defect concentration

refined from the X-ray and neutron diffraction data is now 0.12% (absolute), a superb level of agreement that is small relative to the amount of defects present in the samples (1.5%–5%, absolute). Other choices of X-ray form factors lead to both systematic offsets and larger differences in the defect concentrations refined independently using X-ray and neutron diffraction data (Fig. S8). These results demonstrate that unexpectedly small amounts of structural defects can be identified and robustly quantified with properly corrected powder diffraction data.

The practical advantages of using O^{2-} atomic form factor together with neutral cation atomic form factors in X-ray structural refinements have been established for layered NMC battery compounds, leading to unprecedented sensitivity to defects in this industrially important class of compounds.
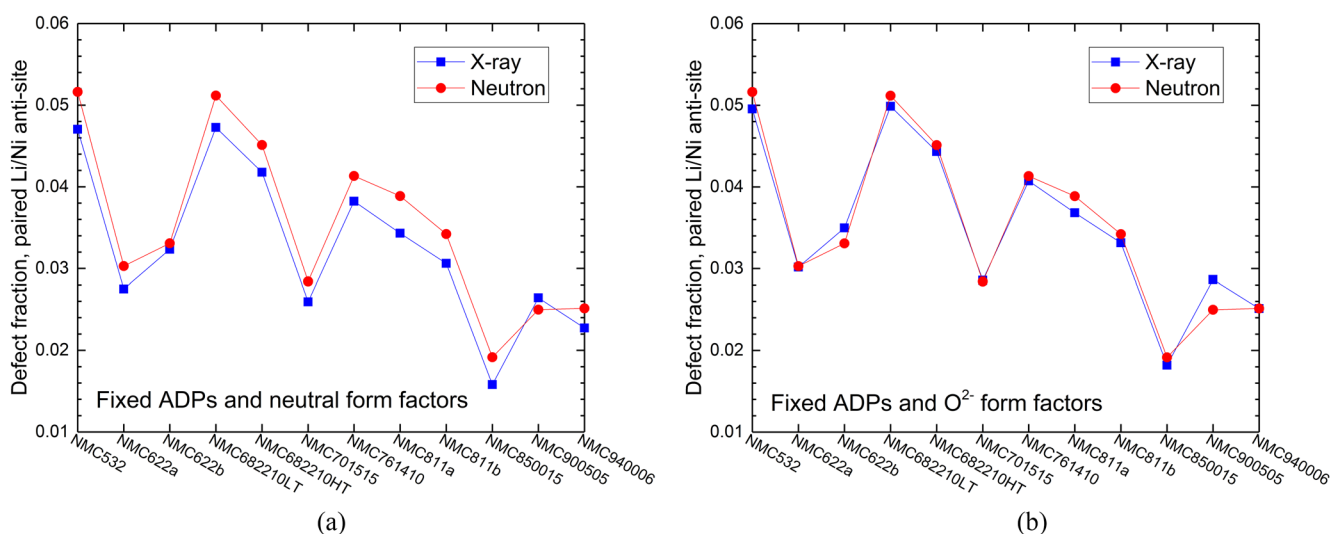

FIG. 10. Comparison of fraction of anti-site defect pairs (Ni_{Li} and Li_{Ni}) refined independently using synchrotron X-ray data (blue) or TOF neutron diffraction data (red) using (a) neutral form factors for all species and (b) ionic form factors for O^{2-} and neutral form factors for all other species. In both cases, ADPs for X-ray refinements were fixed to the values obtained from global refinements against TOF neutron diffraction data. When O^{2-} form factor is used, the systematic offset between X-ray and neutron refinement results is eliminated, resulting in absolute agreements in refined defect concentrations of 0.12%.

It is expected that this approach is generally applicable to structural studies of complex oxides, though further work using the newly developed methodology of f^* diagrams is needed to rigorously evaluate this hypothesis. Despite the experimental success of this approach, theoretical justification for it is presently lacking. The optimal modeling choice can be rationalized if one assumes that the oxygen electron cloud is more strongly perturbed by covalent bonding effects than that of the associated cations. However, nominal expectations for charge balance are not satisfied in this approach, as the O^{2-} species are treated as having two extra electrons relative to their neutral counterparts while the cationic species are not treated as losing any electrons. Furthermore, it can be seen that the ADPs globally refined from synchrotron X-ray data after switching to the O^{2-} ionic form factor substantially differ from those refined from neutron diffraction data (Fig. S9). This behavior can be interpreted as the O^{2-} ionic form factor correctly providing a required net increase in the scattering power at the oxygen site, but incorrectly reproducing the Q-dependence of the oxygen scattering power. It is speculated that the physical origin of the inadequate neutral oxygen form factor is more likely associated with the relatively strong deviations from the assumed aspherical nature of the oxygen electron cloud, a distortion that the cationic species are much less likely to experience. Whether this is the case or not, it is expected that the shape of the oxygen electron cloud may exhibit substantial sensitivity to the nature of bonding, potentially showing resolvable differences between environments with strong covalent bonds (e.g., P–O), in environments which lack covalent interactions (e.g., Li–O), and in environments of intermediate character (e.g., Co–O). Further theoretical and experimental work to better understand the nature of the electron cloud within solid state compounds is merited, and such work should lead to further improvements in the accuracy and confidence in conclusions about site occupancies that can be obtained from powder diffraction data.

It is also noted that the started neutron scattering lengths are typically only reported to 3 significant figures, resulting in possible uncertainties of 0.1%–1%. Although there was no evidence that uncertainty in the literature neutron scattering lengths limited the accuracy of the present work (given the effectiveness of the single-defect models in capturing the global refinement minimum), it seems likely that this uncertainty may be the dominant source of error when other chemical compositions are studied using neutron powder diffraction methods. As such, the technique of powder neutron diffraction appears to have sufficiently advanced to the point where performing higher precision measurements of nuclear scattering lengths will be required to fully unlock the potential of neutron powder diffraction methods to accurately quantify crystallographic site occupancies at with uncertainties of 0.1% or less.

IV. CONCLUSIONS

A comprehensive powder diffraction study of 14 different NMC using high quality synchrotron and time-of-flight neutron diffraction data has been carried out. By eliminating key

correlations and effectively correcting for important experimental aberrations, it is demonstrated that the concentration of ant-site defects in these samples can be independently refined from X-ray and neutron diffraction data with an agreement of 0.1% absolute, an exceptional level of agreement. Furthermore, a new method of visualizing the diffraction parameter space associated with occupancy defects has been described. These f^* diagrams allow the facile discrimination between NMC compounds with one or multiple defects and in many cases provide direct insights into the nature of the defects. Additionally, the f^* diagrams clearly highlight that systematic errors associated with the use of standard neutral atomic form factors to model the synchrotron diffraction data for NMC compounds are associated with the oxygen site. It was found that greatly improved results could be achieved when the scattering from oxygen sites was modeled using the ionic O^{2-} atomic form factor while retaining the neutral form factor for all other species. However, it is likely that even this form factor has limitations and further efforts to model and improve the description of scattering from oxygen anions in complex oxides are merited. The 2-dimensional f^* diagrams used to describe these NMC compounds are broadly applicable to the study of ternary compounds and can also be extended to understand defect concentrations in more complex compounds for which occupancy defects occur over a limited subset of sites in analogy with pseudo-ternary phase diagrams. Although powder diffraction is very susceptible to systematic errors, the approaches presented here offer a new opportunity to understand and eliminate these errors, enabling far more robust and accurate determination of defects present in small concentrations. Furthermore, these methods provide a very accessible pathway to experimentally evaluate atomic scattering factors in compounds beyond unary compounds using either powder or single crystal diffraction data.

SUPPLEMENTARY MATERIAL

See supplementary material for additional tables and figures reporting the results of crystallographic refinements as well as the sample compositions probed by inductively coupled plasma (ICP) analysis techniques, and for sample TOPAS INP control files for carrying out crystallographic refinements of synchrotron and neutron data in the manner described in this manuscript.

ACKNOWLEDGMENTS

[1] P. L. Lee, D. M. Shu, M. Ramanathan, C. Preissner, J. Wang, M. A. Beno, R. B. Von Dreele, L. Ribaud, C. Kurtz, S. M. Antao, X. Jiao, and B. H. Toby, "A twelve-analyzer detector system for high-resolution powder diffraction," J. Synchrotron Radiat. **15**, 427–432 (2008).

[2] J. Neuefeind, M. Feygenson, J. Carruth, R. Hoffmann, and K. K. Chipley, "The nanoscale ordered materials diffractometer NOMAD at the spallation neutron source SNS," Nucl. Instrum. Methods Phys. Res., Sect. B **287**, 68–75 (2012).

[3] V. F. Sears, "Neutron scattering lengths and cross sections," Neutron News **3**(3), 26–37 (1992).

[4] L. Monconduit and L. Croguennec, *Electrodes for Li-Ion Batteries: Materials, Mechanisms and Performance* (John Wiley & Sons, 2015).

[5] T. Ohzuku, A. Ueda, M. Nagayama, Y. Iwakoshi, and H. Komori, "Comparative study of $LiCoO_2$, $LiNi_{1/2}Co_{1/2}O_2$ and $LiNiO_2$ for 4 volt secondary lithium cells," Electrochim. Acta **38**(9), 1159–1167 (1993).

[6] M. S. Whittingham, "Lithium batteries and cathode materials," Chem. Rev. **104**(10), 4271–4302 (2004).

[7] M. Sathiya, G. Rousse, K. Ramesha, C. Laisa, H. Vezin, M. T. Sougrati, M.-L. Doublet, D. Foix, D. Gonbeau, and W. Walker, "Reversible anionic redox chemistry in high-capacity layered-oxide electrodes," Nat. Mater. **12**(9), 827 (2013).

[8] H. Koga, L. Croguennec, M. Ménétrier, K. Douhil, S. Belin, L. Bourgeois, E. Suard, F. Weill, and C. Delmas, "Reversible oxygen participation to the redox processes revealed for $Li_{1.20}Mn_{0.54}Co_{0.13}Ni_{0.13}O_2$," J. Electrochem. Soc. **160**(6), A786–A792 (2013).

[9] Z. Lu, D. MacNeil, and J. Dahn, "Layered cathode materials $Li[Ni_xLi_{(1/3-2x/3)}Mn_{(2/3-x/3)}]O_2$ for lithium-ion batteries," Electrochem. Solid-State Lett. **4**(11), A191–A194 (2001).

[10] Z. Lu, L. Beaulieu, R. Donaberger, C. Thomas, and J. Dahn, "Synthesis, structure, and electrochemical behavior of $Li[Ni_xLi_{1/3-2x/3}Mn_{2/3-x/3}]O_2$," J. Electrochem. Soc. **149**(6), A778–A791 (2002).

[11] Z. Lu and J. R. Dahn, "Understanding the anomalous capacity of $Li/Li[Ni_xLi_{(1/3-2x/3)}Mn_{(2/3-x/3)}]O_2$ cells using *in situ* x-ray diffraction and electrochemical studies," J. Electrochem. Soc. **149**(7), A815–A822 (2002).

[12] J. Dahn, U. von Sacken, and C. Michal, "Structure and electrochemistry of $Li_{1\pm y}NiO_2$ and a new Li_2NiO_2 phase with the $Ni(OH)_2$ structure," Solid State Ionics **44**(1-2), 87–97 (1990).

[13] A. Rougier, P. Gravereau, and C. Delmas, "Optimization of the composition of the $Li_{1-z}Ni_{1+z}O_2$ electrode materials: Structural, magnetic, and electrochemical studies," J. Electrochem. Soc. **143**(4), 1168–1175 (1996).

[14] M. Mendelssohn, "International tables for crystallography. Volume C. Mathematical, physical & chemical tables," Mineral. Mag. **57**(386), 182–184 (1993).

[15] B. Batterman, D. R. Chipman, and J. J. Demarco, "Absolute measurement of atomic scattering factors of iron, copper, and aluminum," Phys. Rev. **122**(1), 68–74 (1961).

[16] S. Hosoya and T. Yamagishi, "Absolute measurement of x-ray scattering factors of copper," J. Phys. Soc. Jpn. **21**(12), 2638–2644 (1966).

[17] M. Diana, G. Mazzone, and J. J. Demarco, "Absolute x-ray measurement of atomic scattering factor of Ni," Phys. Rev. **187**(3), 973–979 (1969).

[18] M. Jarvinen, M. Merisalo, and O. Inkinen, "Absolute measurement of atomic scattering factors of aluminum on powder in transmission," Phys. Rev. **178**(3), 1108–1110 (1969).

[19] M. Diana and G. Mazzone, "Absolute x-ray measurement of atomic scattering factor of chromium," Phys. Rev. B **5**(10), 3832–3836 (1972).

[20] A. Alatas, A. H. Said, H. Sinn, G. Bortel, M. Y. Hu, J. Zhao, C. A. Burns, E. Burkel, and E. E. Alp, "Atomic form-factor measurements in the low-momentum transfer region for Li, Be, and Al by inelastic x-ray scattering," Phys. Rev. B **77**(6), 064301 (2008).

[21] H. Liu, H. Liu, S. H. Lapidus, Y. S. Meng, P. J. Chupas, and K. W. Chapman, "Sensitivity and limitations of structures from x-ray and neutron-based diffraction analyses of transition metal oxide lithium-battery electrodes," J. Electrochem. Soc. **164**(9), A1802–A1811 (2017).